PAPER • OPEN ACCESS

Beyond the quasi-particle: stochastic domain wall dynamics in soft ferromagnetic nanowires

To cite this article: T J Hayward and K A Omari 2017 *J. Phys. D: Appl. Phys.* **50** 084006

View the article online for updates and enhancements.

Beyond the quasi-particle: stochastic domain wall dynamics in soft ferromagnetic nanowires

T J Hayward[1] and K A Omari

Department of Materials Science and Engineering, University of Sheffield, Sheffield, UK

E-mail: T.Hayward@sheffield.ac.uk

CrossMark

Abstract

We study the physical origins of stochastic domain wall pinning in soft ferromagnetic nanowires using focused magneto-optic Kerr effect measurements and dynamic micromagnetic simulations. Our results illustrate the ubiquitous nature of these effects in $Ni_{80}Fe_{20}$ nanowires, and show that they are not only a result of the magnetisation history of the system (i.e. the magnetisation structure of the injected domain walls), and the onset of non-linear propagation dynamics above the Walker breakdown field, but also a complex interplay between the two. We show that this means that, while micromagnetics can be used to make qualitative predictions of the behaviour of domain walls at defect sites, making quantitative predictions is much more challenging. Together, our results reinforce the view that even in these simple pseudo-one dimensional nanomagnets, domain walls must be considered as complex, dynamically evolving objects rather than simple quasi-particles.

Keywords: domain wall, stochastic, nanomagnets, racetrack memory, domain wall logic

S Supplementary material for this article is available online

(Some figures may appear in colour only in the online journal)

Introduction

The behaviour of domain walls (DWs) in soft ferromagnetic nanowires [1] has been a topic of intense research since proposals for using DWs to represent data in non-volatile and solid state logic [2, 3] and memory [4, 5] devices were made around the turn of the century. In these devices, it was proposed that trains of DW quasi-particles would be propagated through extended nanowires containing geometrical features at speeds of many hundreds of ms^{-1} either using applied magnetic fields [6] or spin torque effects [7], thus allowing data to be written, read and processed.

Despite the technological promise of DW devices, and a huge amount of research dedicated to their development, they have yet to be commercially realised (with a few specialised exceptions [8]). This is primarily due to two inhibiting factors: Firstly, in soft ferromagnetic materials such as $Ni_{80}Fe_{20}$, it is difficult to propagate DWs efficiently, with current densities $\sim 10^{13}$ Am^{-2} being required to move DWs with spin torque effects at velocities $\sim 100\,ms^{-1}$ [9]. Similar velocities may also be achieved using applied fields [6], but such an approach is limited by the current densities required to create sufficient magnetic fields over the scale of a device, and the practical difficulties in obtaining unidirectional DW motion with an applied field [10]. A second problem is the anomalously high stochasticity of DW motion, which manifests as an inability to accurately predict the response of a DW to an applied impulse. For example, DW transmission through nominally defect free nanowires has been shown to be probabilistic even for fields much greater than those required to initiate DW propagation

[11–13]. Furthermore, artificial DW pinning sites that are introduced to stabilise DW positions have complex, multi-mode depinning field distributions [11, 14–18], and may be passed probabilistically even when DWs are propagated by applied fields that would nominally be insufficient to induce depinning [11, 16, 19, 20].

Recently it has been shown that more efficient DW motion can be obtained in nanowires fabricated from ultra-thin layers with perpendicular magnetic anisotropy (PMA). For example, in multilayers such as $Pt/Co/AlO_2$ that exhibit interfacial Dzyaloshinsky–Moriya interactions, DWs adopt chiral structures that can be propagated efficiently using the spin Hall effect [5]. The DWs formed in these materials are narrow, and have simpler spin structures than those observed in nanowires with in-plane anisotropy (IPA). This makes them less susceptible to complex stochastic pinning effects such that, from the perspective of device development, moving to more advanced materials systems overcomes two of the major obstacles to commercial realisation simultaneously.

Despite this, the anomalous stochastic pinning and propagation behaviours of DWs in nanowires with IPA remain interesting phenomena to study at a fundamental level, and are highly important to the dynamics of more complex nanomagnet ensembles such as Kagome artificial spin ice lattices [21, 22]. Furthermore, while the complex spin structures of DWs in IPA nanowires lie at the heart of stochastic pinning behaviours [14], their interactions with geometric features create novel functionalities that cannot be replicated in PMA systems [3]. Therefore, developing a comprehensive understanding of the stochastic pinning of DWs in IPA nanowires remains an interesting and relevant problem.

In this paper we will first provide an extended introduction to stochastic pinning phenomena in magnetic nanowires devices using the results of both experimental measurements and micromagnetic simulations. These results will illustrate how stochastic DW pinning effects manifest, demonstrate their ubiquitous nature in $Ni_{80}Fe_{20}$ nanowires, and explain our current understanding of their physical origin. We will then present a new micromagnetic-based modelling protocol that exploits this understanding to allow qualitative predictions of a given defect site's depinning field distributions to be made. Finally, we will present results showing that the quantitative degree of stochasticity observed at a defect site fundamentally depends on method by which DWs are nucleated into a nanowire. This indicates that stochastic pinning is not only caused by the magnetisation history of the nanowires and the propagation dynamics of DWs within them, but also a complex interplay between the two. This additional layer of complexity further demonstrates the necessity of considering DWs in nanowires as complex, dynamically evolving systems, rather than as rigid quasi-particles.

Experimental techniques

$Ni_{80}Fe_{20}$ nanowires widths of $w = 400$ nm and thicknesses in the range $t = 10$–40 nm were patterned using electron-beam lithography and lift-off processing, and metallised by thermal evaporation at a base pressure of ~10^{-7} mbar. In some devices

nucleation pads were added to the ends of the nanowires in order to facilitate the injection of DWs with externally applied magnetic fields, while in other devices 4 μm wide Ti (20 nm)/Au (200 nm) orthogonal strip lines were patterned close to the end of the nanowires via optical lithography. In these latter devices DWs were injected by the localised Oested field created when ~50 ns long current pulses (current density ~10^{11} Am^{-2}) were passed through the strip lines using a nanosecond pulse generator. This allowed precise control of the conditions under which DWs were introduced into the nanowires. In order to study DW pinning, notch-shaped defect sites with depths (d_N) in the range 15%–75% of the nanowires' widths were patterned into the nanowires. In all cases, the widths of the notches were equal to their depths.

The nanowires' switching behaviours were probed using a focused magneto-optic Kerr effect (FMOKE) magnetometer with a probe laser spot size ~3 μm. Sinusoidally varying magnetic fields with amplitudes up to 600 Oe were applied to the samples via a quadrupole electromagnet, and were swept continuously at a frequency of 27 Hz during measurements. The sensitivity of the FMOKE was sufficient that individual magnetic reversals of the nanowires could be measured. This capability was used to investigate the stochasticity of the nanowires' switching by performing ~100–200 single shot measurements both before and after the notch-shaped defect sites. This allowed DW injection field (IFD) (i.e. that required to move a DW from a pad to a notch) and depinning field (DFD) (i.e. that required to depin a DW from a notch and sweep it out a nanowire) distributions to be measured for each of the devices studied. In the majority of the nanowire devices the fields at which DWs were injected was dictated by the relatively wide switching fields of nucleation pads. However, in the devices with strip lines synchronisation of the current pulses to the applied field sweep of the electromagnet allowed the DW injection fields to be precisely controlled. A schematic diagram indicating the measurement geometry and the basic switching behaviour of the nanowire devices is shown in figure 1.

Micromagnetic simulations of the nanowires were performed using the Mumax^3 software package [23]. Cell sizes of $2.5 \times 2.5 \times 2.5$ nm^3 or $2.5 \times 2.5 \times 5$ nm^3 were used depending on how finer a mesh was required to achieve convergence of the DW dynamics. Standard values [24] were used to model the material parameters of the nanowires: Saturation magnetisation $M_s = 860$ kAm^{-1}, exchange constant $A = 13$ pJ m^{-1} and magnetocrystalline anisotropy constant $K_1 = 0$. For dynamic simulations (e.g. of DW propagation) realistic damping constants in the range $\alpha = 0.01$–0.02 were used, while for quasi-static simulations (e.g. to determine DW depinning fields) larger values in the range $\alpha = 0.5$–1 were used to reduce simulation times.

Stochastic pinning/depinning behaviour

In this section of the paper we will present experimental measurements from a range of magnetic nanowire devices to provide the reader with an introduction to stochastic DW pinning phenomena, and to demonstrate their ubiquitous nature.
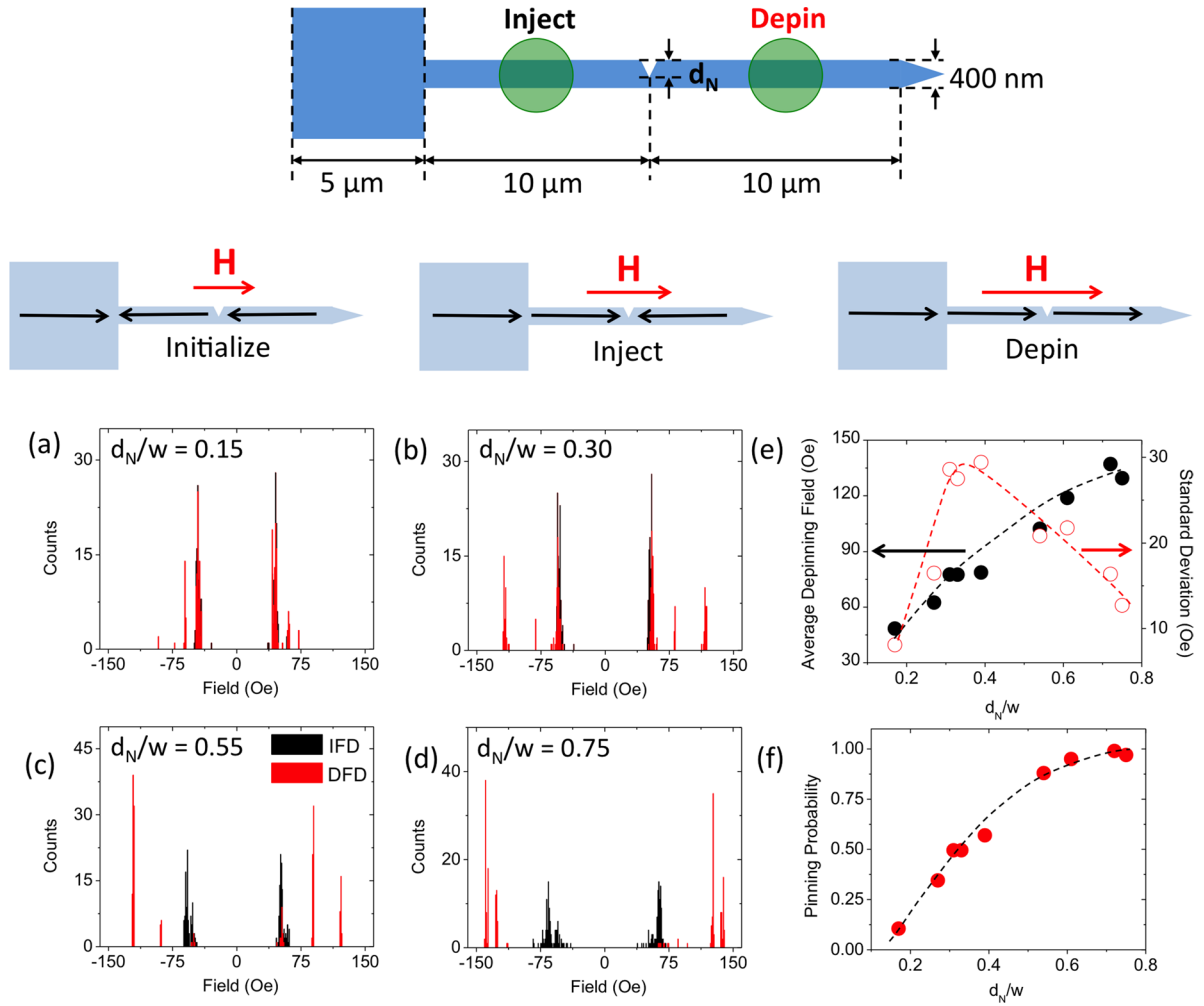
Figure 1. Characterisation of the IFDs and DFDs of nanowires containing single notch defects. Schematic diagrams of the experiment geometry and nanowires' switching sequences are shown at the top of the figure. (a)–(d) IFDs (black) and DFDs (red) measured for nanowires with d_N/w equal to (a) 0.15, (b) 0.30, (c) 0.55 and (d) 0.75. (e) Plots showing the mean depinning field (closed circles) and standard deviation of the DFDs (open circles) as a function of d_N/w. (f) Plot showing the pinning probability of the DWs as a function of d_N/w.

In order to explore the extent of stochastic DW pinning/depinning at defect sites in $Ni_{80}Fe_{20}$ nanowires a range of devices with $w = 400\,nm$ and $t = 10\,nm$, 25 nm or 40 nm were characterised using FMOKE measurements. Nanowires containing both single- and double-notch defects, with a range of depths, were studied.

Figures 1(a)–(d) presents example IFDs and DFDs measured from $t = 25\,nm$ nanowires containing single notch defects with depths in the range $d_N/w = 0.15$–0.75. Each of the devices studied exhibited relatively broad IFDs centred on a central peak in the range 45–65 Oe, with the slight differences from one device to the next being accounted for by lithographic imperfections at the junction between the pad and the nanowire. In contrast, the DFDs had much more complicated characters that illustrate both of the characteristic features of stochastic DW pinning/depinning: Firstly, in all four devices, the DFDs exhibited two clear peaks (or modes), indicating that pinned DWs could depin from the defect sites in at least two distinct ways. Secondly, there was substantial overlap between the IFDs and DFDs, indicating that many of the DWs passed straight through the defect sites without

pinning. These features have been observed consistently across many distinct studies of DW behaviour [14–20]. We note that the slight asymmetries in the amplitudes of the DFD peaks for the forward and reverse field sweeps can be explained by either history dependent magnetic switching, reflecting the modest amplitude of our saturating field (600 Oe), or by sample tilts of a few degrees, both of which could be expected to slightly bias the chiralities of injected DWs. Intrinsic differences between the depinning mechanisms of head-to-head and tail-to-tail DWs would not be expected.

In order to quantify the depinning behaviour three numerical metrics were measured from the DFDs of a larger sample of nanowire devices: the mean depinning field, the standard deviation of the DFD and the pinning probability (as defined by the fraction of depinning events that did not overlap with the IFD). These metrics are plotted as a function of notch depth in figures 1(e) and (f), and show that, despite the apparent complexity of the DFDs, some clear trends can be identified. For example, both the mean depinning field and pinning probability increased with the notches' depth, due to the increased size and gradient of the potential barriers these created against DW
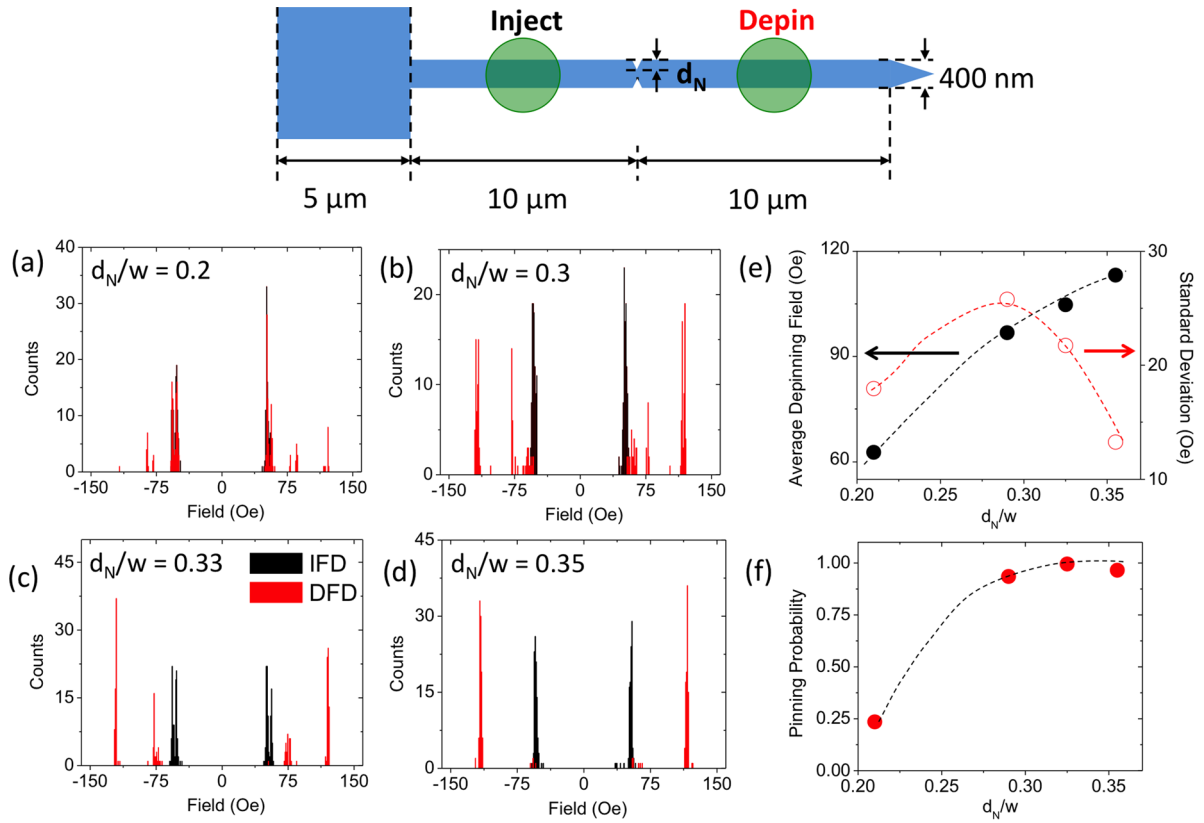
Figure 2. Characterisation of the IFDs and DFDs of nanowires containing double notch defects. (a)–(d) IFDs (black) and DFDs (red) measured for nanowires with d_N/w equal to (a) 0.20, (b) 0.30, (c) 0.33 and (d) 0.35. (e) Plots showing the mean depinning field (closed circles) and standard deviation (open circles) of the DFDs as a function of d_N/w. (f) Plot showing the pinning probability of the DWs as a function of d_N/w.

propagation (we further note that these two parameters would not be expected to be entirely independent of each other, as for the DWs that did not pin the depinning field was equivalent to the injection field, thus reducing its mean value at lower pinning probabilities). The standard deviation of the distribution showed a more complex trend, rising to a peak at $d_N/w \sim 35\%$, before decreasing again. We note that this behaviour was not simply due to the shift from most DWs passing the pinning site to most DWs pinning at it, which would be expected to cause a peak at approximately 50% pinning probability, because the same trend was also observed when only considering events where the DWs pinned. Instead the peak in σ was due to a combination of factors including the spread of the modes' depinning fields and the degree to which they were populated.

While the multi-mode DFDs shown in figure 1 are complex, they are compatible with a relatively simple picture of DW stochasticity. It is well-known DWs exhibit chirality dependent interactions with asymmetric defect sites, such that a single-notch defect will exhibit different depinning fields for clockwise (CW) and anticlockwise (ACW) vortex DWs (VDWs), or for up and down magnetised transverse DWs (TDWs) [14]. In $t = 25$ nm, $w = 400$ nm nanowires it is expected that VDWs will be energetically favoured [24] and thus the observation of bimodal DFDs could potentially be explained by a mixture of CW and ACW VDWs being injected from the nucleation pads and propagating rigidly to the notch. However, measurements in further devices clearly show this to provide an incomplete picture.

Following the logic above, one would expect that symmetric double-notch defect sites would suppress chirality-dependent pinning effects and thus produce simple, single-mode DFDs. To probe this, IFDs and DFDs were measured for nanowires containing double-notch defects with d_N/w in the range 0.2–0.35 (figures 2(a)–(d)). With the exception of the nanowire with the largest notches ($d_N/w = 0.35$), which exhibited a well-defined single mode DFD, all of the other nanowires showed complex DFDs consisting of a least two modes, much like those of the nanowires with single notches. This similarity between the DFDs measured for single and double notch geometries was further reflected in the quantitative metrics measured for the double-notch defects (figures 2(e) and (f)), with the mean depinning field and pinning probability increasing with notch size, and a non-monotonic trend being observed for σ. The observation of complex stochastic behaviours, even for non-chirality-sensitive defect sites, clearly demonstrates that their origin was not simply a lack of control of the chirality of the DWs that were introduced into the nanowires.

Thus far we have presented data from only one device (figure 2(d)), where DW pinning was relatively reliable (pinning probability = 0.956) and depinning occurred via a single well-defined mode. This reflects the ubiquitous nature of stochastic effects in DW devices, with geometries that exhibit well-defined behaviour being the exception rather than the rule. We further emphasise this in figure 3 which compares
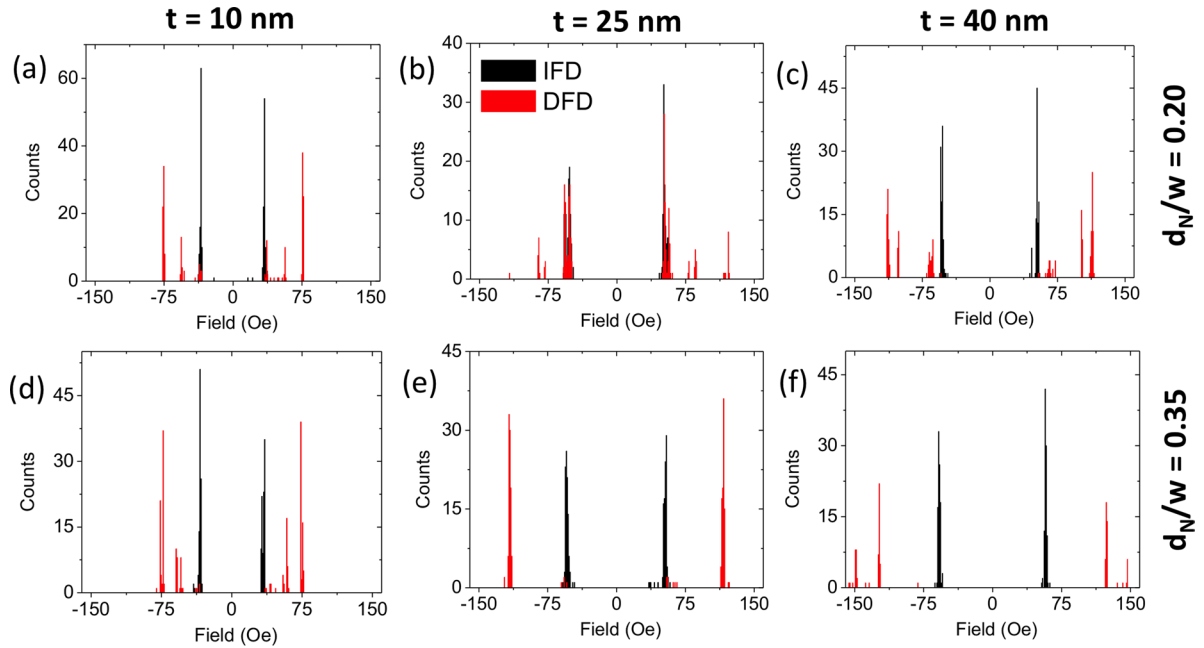
Figure 3. Characterisation of the IFDs and DFDs of nanowires of various thicknesses containing double notch defects. (a)–(c) Notches have $d_N/w = 0.2$, and nanowire thickness equal to (a) 10 nm, (b) 25 nm, (c) 40 nm. (d)–(f) Notches have $d_N/w = 0.35$, and nanowire thickness equal to (d) 10 nm, (e) 25 nm, (f) 40 nm.

IFDs and DFDs for two geometries of double-notch defect sites ($d_N/w = 0.20$ and 0.35) in nanowires with $t = 10$ nm, $t = 25$ nm and $t = 40$ nm. With the exception of the geometry identified previously ($t = 25$ nm, $d_N/w = 0.35$), all of the nanowires exhibit complex multimode DFDs and/or pinning probabilities <1. We note that, while the results presented here explore a relatively small window in phase space, our statement that stochastic pinning is a generalised phenomena in soft-ferromagnetic nanowires is further supported by numerous studies in the literature where these effects have been observed over a wide range of nanowire and notch geometries [14–20].

The data presented so far has focused on the pinning and depinning of DWs from artificially patterned defect sites. However, lithographically patterned nanowires will always have a finite degree of edge roughness that can also pin DWs. Studying the interaction of DWs with these defect sites is more difficult than in systems with well-defined artificial notches, however several authors have presented studies that have demonstrated how stochastic pinning at these defects results in probabilistic DW propagation even under fields as large as several tens of Oested [11–13].

In figure 4 we present experimental data illustrating the effects of stochastic pinning in nominally defect free nanowires. In these experiments DW pairs were injected into a $t = 20$ nm, $w = 400$ nm by supplying a voltage pulses to an orthogonal current line patterned over the end of the nanowire. The applied field was then ramped such that one of the DWs was driven out of the nearest end of the nanowire, while the other was propagated along it. FMOKE measurements were then used to characterise the DWs' propagation fields at positions 4, 8, 12 and 16 μm from the current line's edge. A schematic diagram of the experimental setup is shown in figure 4(a).

Figure 4(a) presents histograms of the propagation field distributions measured at each of the locations along the nanowire. Each histogram exhibits a wide distribution of propagation fields, demonstrating the stochastic nature of the DWs' propagation. The distributions both broaden and shift towards higher fields as the distance along the nanowire increases, features that are illustrated more clearly in figures 4(b) and (c) where the mean propagation field and the standard deviation of the distribution are plotted as a function of distance. Of particular note is the large range of fields observed at a single point. For example, at 16 μm from the current line, propagation fields as low as 16 Oe and as high as 57 Oe are observed, showing that even relatively small edge defects can add significant levels of unpredictability to DW motion. Furthermore, the data provides additional evidence that a mixture of rigid DW structures (e.g. ACW and CW VDWs) being injected into the nanowires cannot explain stochastic DW pinning in isolation. Were this to be the case two clear modes would be observed in the DFDs, corresponding to ACW and CW VDWs depinning from the defect sites that pin their respective chiralities most strongly. Clearly a more sophisticated model of DW pinning must be developed.

Dynamic domain wall pinning

In the previous section we presented experimental results that illustrated the ubiquitous nature of stochastic DW pinning in soft ferromagnetic nanowires, and demonstrated why these effects cannot be caused purely by DWs being injected with poorly defined chiralities. In this section we will present the results of micromagnetic simulations that illustrate the importance of the complex internal magnetisation dynamics of propagating DWs to stochastic pinning phenomena
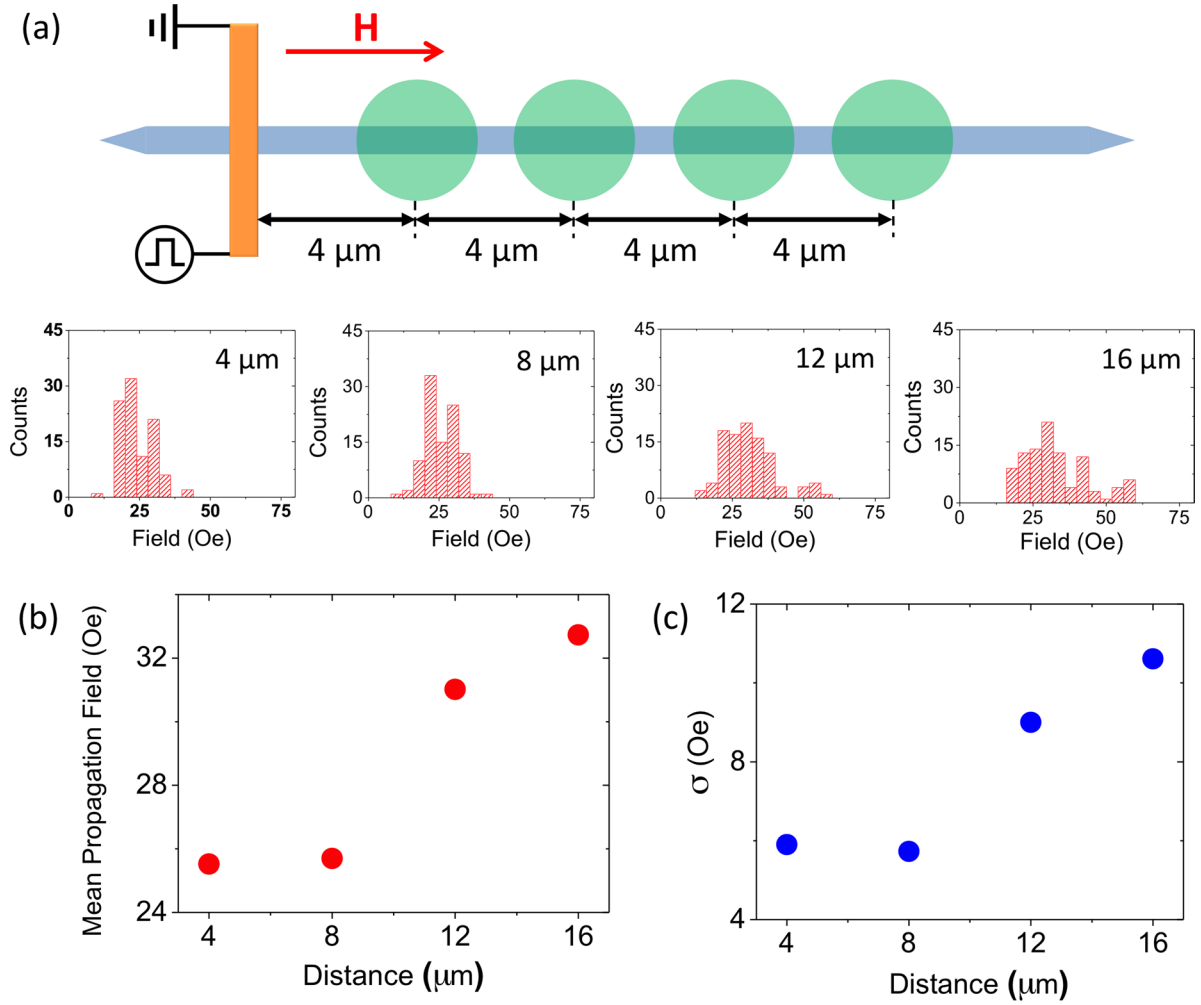
J. Phys. D: Appl. Phys. **50** (2017) 084006

T J Hayward and K A Omari

Figure 4. Characterisation of DW propagation fields as a function of distance along a $t = 20$ nm, $w = 400$ nm nanowire. (a) Propagation field distributions measured at 4 μm, 8 μm, 12 μm and 16 μm from the injection current line. A schematic diagram of the experimental geometry is also shown. (b) Mean propagation field plotted as a function of distance. (c) Standard deviation of the distribution plotted as a function of distance.

[11–13, 16, 20], and thus enable us to understand the sources of the stochasticity observed in our experimental measurements.

Figure 5(a) shows plot of average DW velocity versus applied field as obtained from micromagnetic simulations of a $t = 25$ nm, $w = 400$ nm nanowire ($\alpha = 0.02$). The data shows the characteristic shape expected for DWs in planar, soft ferromagnetic nanowires [6], with two clear regimes of DW motion separated by a critical field value known as the Walker breakdown field [26], H_{WB}. For $H < H_{WB}$ the DW velocity increases linearly with applied field, while for $H > H_{WB}$ the DW velocity drops and remains relatively constant over the simulated field range.

At a nanomagnetic level the two regimes of motion are differentiated by the internal dynamics of the propagating DWs: Below H_{WB} DWs are transported with rigid magnetisation structures, while above H_{WB} their structures oscillate between different configurations. This is illustrated in figure 5(c), which contrasts the magnetisation dynamics of DWs at $H = 12.5$ Oe ($<H_{WB}$) and 30 Oe ($>H_{WB}$). At $H = 12.5$ Oe the DW retained both its basic VDW character and ACW chirality as it propagated. However, at $H = 30$ Oe the DW periodically

oscillated between VDW and a pseudo-TDW structure where the vortex core resided close to the edge of the nanowire. The effects of Walker breakdown can also be seen clearly in figure 5(b), which plots the positions of DWs as a function of time for a variety of fields. At $H = 30$ Oe and $H = 40$ Oe, fields which both lie above H_{WB}, the transformations of DW structure caused short periods of retrograde motion that lowered the DWs' time-averaged velocities and give the curves a characteristic oscillating form.

Several authors have identified this transient nature of DW structure when propagating above H_{WB} as the underlying cause of stochastic pinning phenomena [11–13, 16, 20]. In these models Walker breakdown causes DWs to arrive at defect sites with a variety of magnetisation configurations, and thus pin in a variety of distinct states. For example, figure 5(d) shows the final states of simulations where DWs were propagated at $H = 50$ Oe to $d_N/w = 0.25$ single notches placed at different positions along a nanowire. Because the notches interrupted the regular sequence of Walker breakdown transitions at different points, both TDW and VDW configurations were pinned. In general different DW configurations
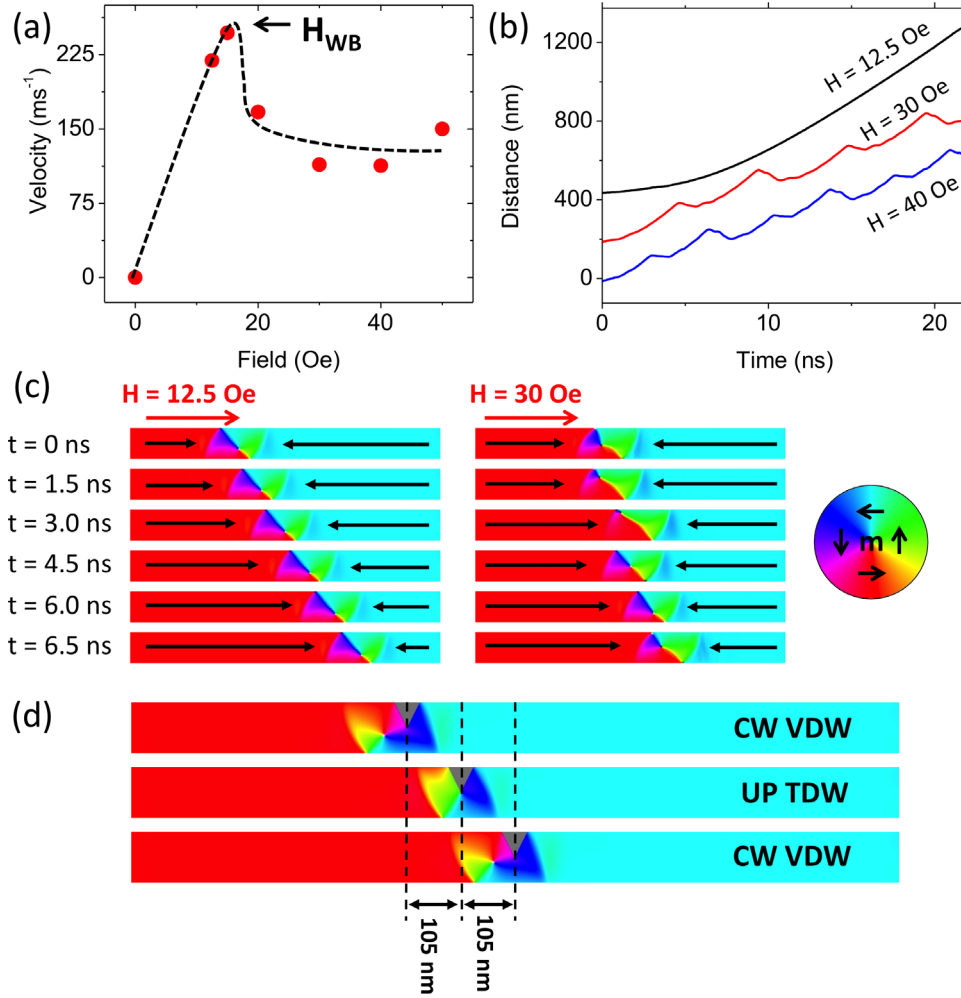
Figure 5. Micromagnetic simulations of domain wall propagation dynamics in a $t = 25$ nm, $w = 400$ nm nanowire. (a) Plot of average domain wall velocity as a function of applied field. The Walker breakdown field, H_{WB}, is indicated. (b) Plots of domain wall position versus time for $H = 12.5$, 30 and 40 Oe. (c) Comparisons of domain wall dynamics at $H = 12.5$ Oe (below H_{WB}) and $H = 30$ Oe (above H_{WB}). (d) Domain wall states pinned at $d_N/w = 0.5$ single notches placed at different locations in a nanowire following propagation at $H = 50$ Oe.

will have different depinning fields, thus leading to the multimode DFDs observed in experimental studies of DW behaviour. Furthermore, DWs arriving at specific points in their transformation sequence are able to pass through defect sites that would normally be expected to pin them, thus leading to probabilistic DW pinning [11, 15, 20]. Thus, both of the primary features of stochastic DW pinning can be caused by the complex magnetisation dynamics of DWs propagating above H_{WB}.

We note that the dynamic model of stochastic pinning can also explain the apparent ubiquitous presence of stochastic pinning in experimental characterisations of DW behaviour: H_{WB} is typically <25 Oe for most nanowire geometries (e.g. [6, 11]) and therefore usually lies both below the fields at which DWs are typically nucleated from injection pads (e.g. figures 1(a)–(d)), and within the range of typical propagation fields (e.g. figure 4(a)). This means that, in experiments, DWs are almost always propagating with transient structures, and thus would be expected to exhibit stochastic pinning. Furthermore, in particularly well-controlled experiments where DWs have been reliably transported at fields below H_{WB} stochastic pinning has been seen to be suppressed [13, 16].

Qualitative modelling of stochastic DW pinning

In the previous section we used micromagnetic simulations to illustrate that the stochastic pinning of DWs can be explained by the complex magnetisation dynamics of DWs propagating above H_{WB}. In this section we will exploit this understanding by applying a new micromagnetic-based modelling protocol to explain the physical origin of the DFDs observed for the $t = 25$ nm, $w = 400$ nm nanowires characterised in the first part of this paper.

Our simulation methodology proceeded as follows: We began by making the assumption that DWs propagating at a given field would exhibit a finite range of interactions with defects, based on the internal magnetisation configurations they pass through during a single Walker breakdown cycle. To examine these interactions we first simulated the dynamics of DWs propagating through the system at the average injection field of the nanowires and measured the distance propagated in one complete cycle. Further simulations were then performed with notches placed at each of 10 regularly spaced positions within the cycle distance in order to characterise how the DWs would interact and pin at the defects at each point in their
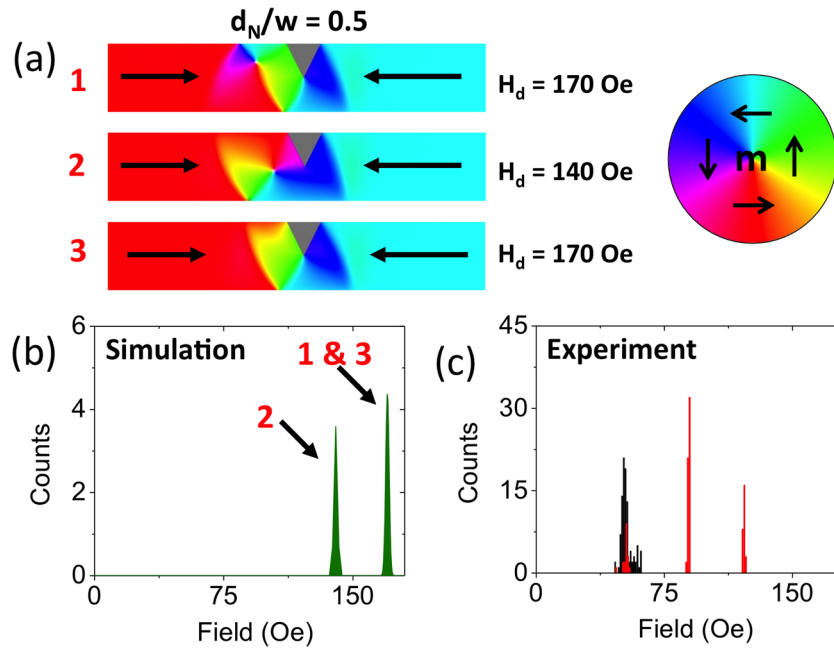
Figure 6. (a) Micromagnetic simulations of possible pinned domain wall states in a $t = 25\,\text{nm}$, $w = 400\,\text{nm}$ nanowire with a $d_N/w = 0.5$ single notch. The depinning field of each state is also listed. (b) DFD derived from the micromagnetic simulations. The domain wall states that contribute to each peak are indicated. (c) Experimentally measured IFD (black) and DFD (red) from a nanowire with a notch identical to the simulated geometry.

transformation cycle. Finally, quasi-static simulations were performed to determine the depinning field, H_d, of each of the pinned states. This simulation process was repeated for both chiralities of the ground state DW configuration, in order to take account of the fact that the chirality of the injected DWs was not controlled in our experiments.

For the $t = 25\,\text{nm}$, $w = 400\,\text{nm}$ nanowires, the average DW injection fields were typically ~50 Oe. A transformation cycle was found to take ~7 ns, with the DW propagating ~1050 nm during this time. A total of 10 simulations were therefore performed with notches placed at 105 nm intervals along the nanowire for both ACW and CW VDW initial states in order to determine the range of possible pinned DW states.

In figure 6 we present results obtained when this simulation method was applied to a single notch with depth $d_N/w = 0.5$. The pinned DW states we observed are shown in figure 6(a), and comprised of VDWs with both chiralities and TDWs with 'up' magnetisation. The ACW VDWs and 'up' TDWs depinned at $H_d = 170$ Oe by very similar mechanisms, while the CW VDWs depinned at the lower field of $H_d = 140$ Oe. Figure 6(b) shows a model DFD derived from this data by assigning each individual depining mode a discrete Gaussian DFD with $\sigma = 1$ Oe and an amplitude scaled to the mode's occurrence in the pinning simulations. Two clear and well-separated depinning modes may be observed. This can be compared to figure 6(c), which presents the IFD and DFD measured experimentally from a nanowire containing a notch of the same geometry. While the quantitative values of the depinning fields are lower than in the simulations (as would be expected for measurements at finite temperature), the experimental and simulated DFDs are qualitatively very similar, allowing us to interpret the two depinning modes observed

experimentally as being due to the pinning of both chiralities of VDWs and a single chirality of TDW at the notch.

In figure 7(a) we present the results of applying the same modelling procedure to a double notch with $d_N/w = 0.2$. As discussed earlier, the experimental DFDs for this symmetric defect are puzzling as, neglecting the events where DWs did not pin, it exhibited two groups of depinning modes despite the fact that the notch should be insensitive to DW chirality. Again, good qualitative agreement between the experimental and simulated DFDs was observed, with two distinct peaks also being present in the derived DFD. The simulations suggest that splitting of the DFD was in fact due to VDWs pinning in slightly different positions, either before the notch (configurations 1 and 3, $H_d = 185$ Oe), or with the VDWs' leading edges protruding though it (configurations 2 and 4, $H_d = 145$ Oe), thus creating the two distinct peaks observed experimentally.

Figure 7(b) presents results for a larger double notch with $d_N/w = 0.35$, which was the only geometry in the experimental measurements to exhibit a DFD consisting of a single well-defined mode. This single mode behaviour ($H_d = 170$ Oe) is replicated in the simulated DFD, despite the fact that four distinct pinned DW configurations equivalent to those found for $d_N/w = 0.2$ are observed. The collapse of the DFD to a single depinning mode for this geometry can therefore be ascribed to a contraction towards a single depinning mechanism, rather than to the notch supporting a limit number of pinned states. We note that this contraction to a single mode was not observed for other nanowire thicknesses (see figure 3), further illustrating the complex geometrical dependence of DW-defect interactions.

The strong agreement obtained between the experimentally measured and simulated DFDs demonstrates the power of this
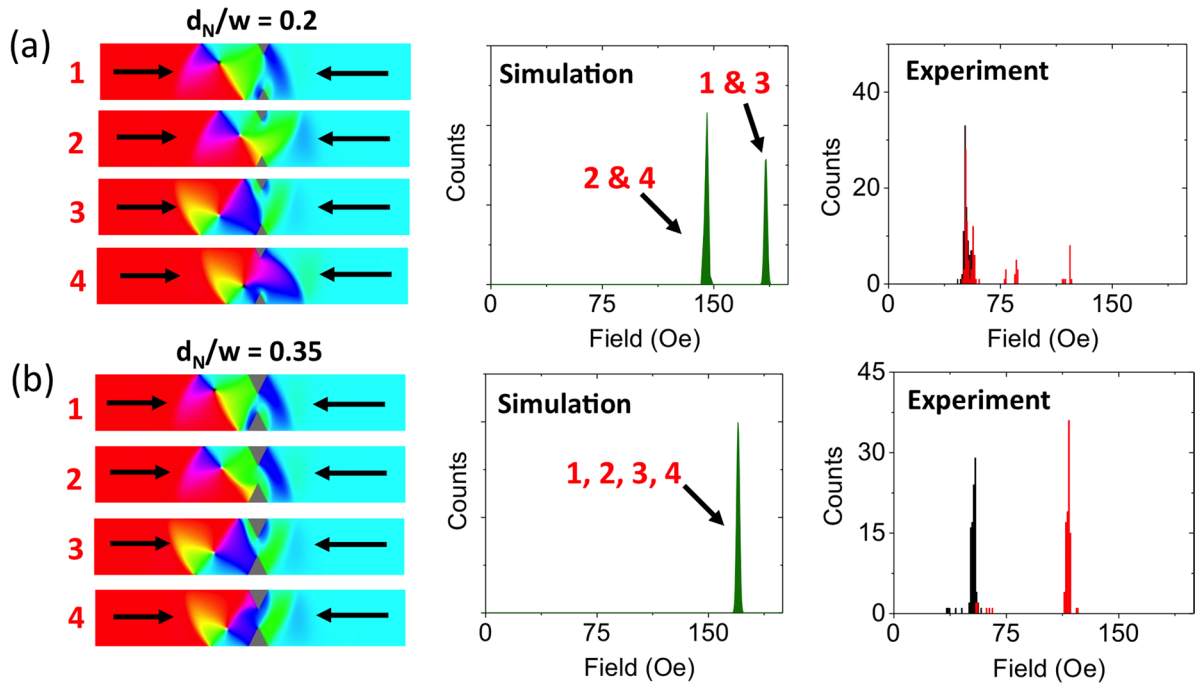
Figure 7. (a) Micromagnetic simulations of possible pinned domain wall states and a derived DFD for a $t = 25\,\text{nm}$, $w = 400\,\text{nm}$ nanowire with a $d_N/w = 0.2$ double notch. Experimentally measured IFDs (black) and DFDs (red) from a nanowire with a notch identical to the simulated geometry are also shown for comparison. (b) Equivalent simulation and measurements for a nanowire with a $d_N/w = 0.35$ double notch.
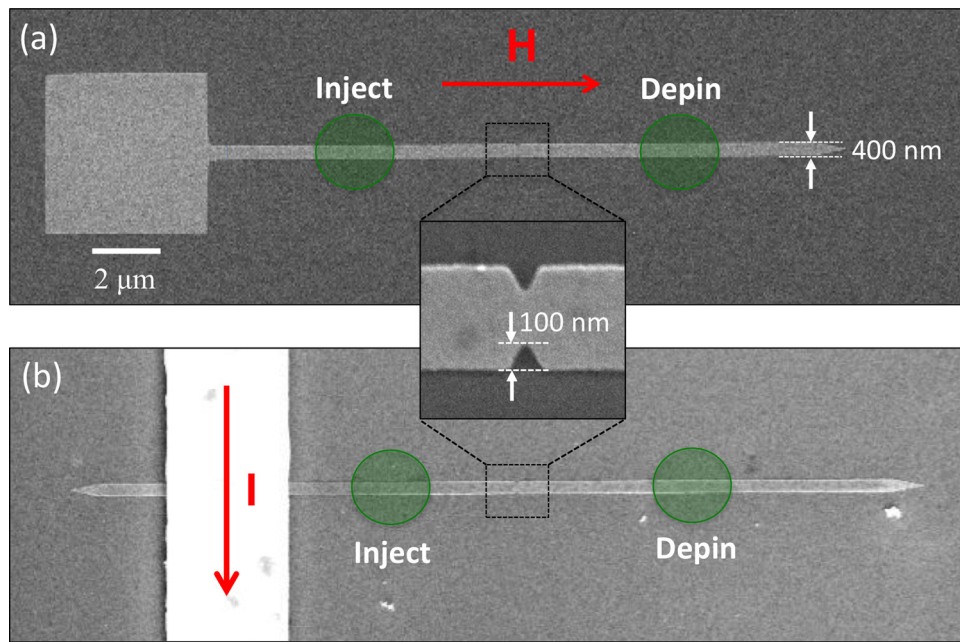

Figure 8. Scanning electron microscope images of example devices used to probe the effects of the domain wall injection method on stochastic pinning/depinning. (a) Nanowire with a nucleation pad. (b) Nanowire with an orthogonal current line. The inset image shows an enlargement of the notch geometry used in the experiment.

modelling approach to explain stochastic pinning at a qualitative level.

Nucleation dependent stochastic pinning behaviour

The results presented thus far clearly show that a qualitative understanding of stochastic DW pinning effects requires consideration of the magnetisation dynamics of propagating

DWs, rather than simply the variations in the magnetisation history of the system (e.g. a mixture of ACW and CW VDWs being injected into a nanowire). However, it is also important to study interplay between these two potential sources of stochasticity if we are to obtain a more quantitative understanding. For example in the experimental measurements presented in figures 1 and 2, DWs were introduced into the nanowires from extended nucleation pads with relatively
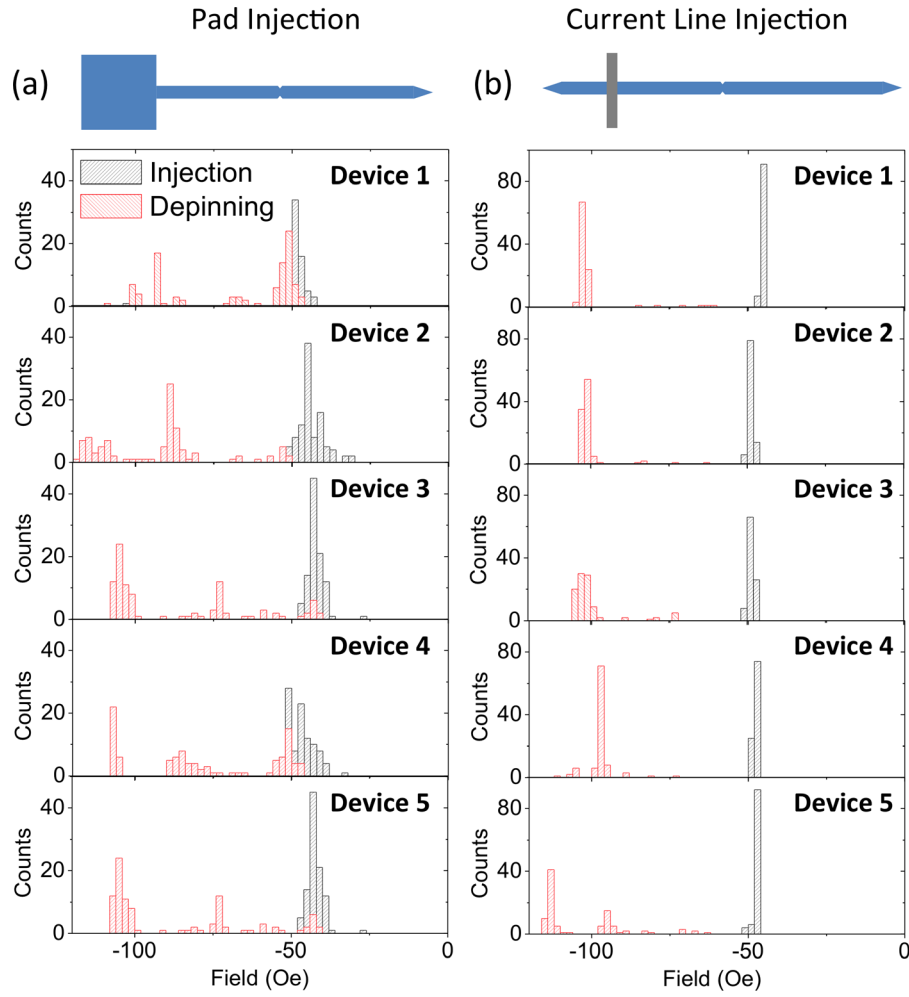
Figure 9. (a) IFDs (black) and DFDs (red) measured from five nominally identical $t = 20$ nm, $w = 400$ nm nanowires containing $d_N/w = 0.25$ double notches, where domain walls were injected from nucleation pads. (b) Equivalent data for five nominally identical nanowires where domain walls were injected from current lines. In all cases the numbers ascribed to the devices are arbitrary and are not intended to indicate correlation between particular devices.
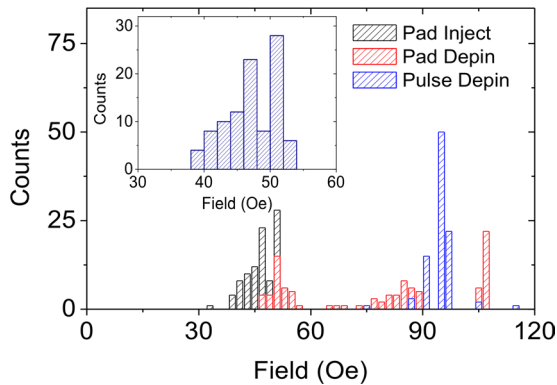

Figure 10. Comparison between the DFDs obtained for a nanowire with nucleation pad (red), and a nanowire with a current line (blue) that was used to mimic the IFD of the nucleation pad (black). The inset figure shows the weighted IFD obtained from the current line devices.

broad IFDs. It was therefore interesting to examine whether the stochasticity of DW pinning/depinning could be reduced if more controlled methods of DW injection were used.

To probe this we fabricated two sets of $t = 20$ nm, $w = 400$ nm nanowires containing double notches with $d_N/w = 0.25$.

In the first set of devices DWs were injected via 5 μm × 5 μm nucleation pad as in the previous experiments (figure 8(a)). In the second set DW injection was achieved by supplying a current pulse to a current line patterned orthogonally over the end of the nanowires (figure 8(b)). The resulting current pulse was synchronised with the applied field, such that DWs were injected into the nanowires at the mean field of injection from nucleation pads (−48 Oe). Scanning electron microscope imaging showed the notches in the two sets of nanowires to be close to identical with mean gap widths of 235 ± 5 nm (standard deviation = 10 nm) in the current line wires and 246 ± 3 nm (standard deviation = 6 nm) in the nucleation pad wires. Furthermore, we note that the use of chirality insensitive double-notch defects in this experiment ensured that the results were not biased by one of our injection methodologies preferentially introducing VDWs of a single chirality into the nanowires. FMOKE measurements were used to characterise the nanowires' IFDs and DFDs over a 100 single shot measurements. A total of five devices were measured for each injection method.

Figure 9 compares the IFDs and DFDs from the nanowires with nucleation pads (figure 9(a)) to those from the nanowires
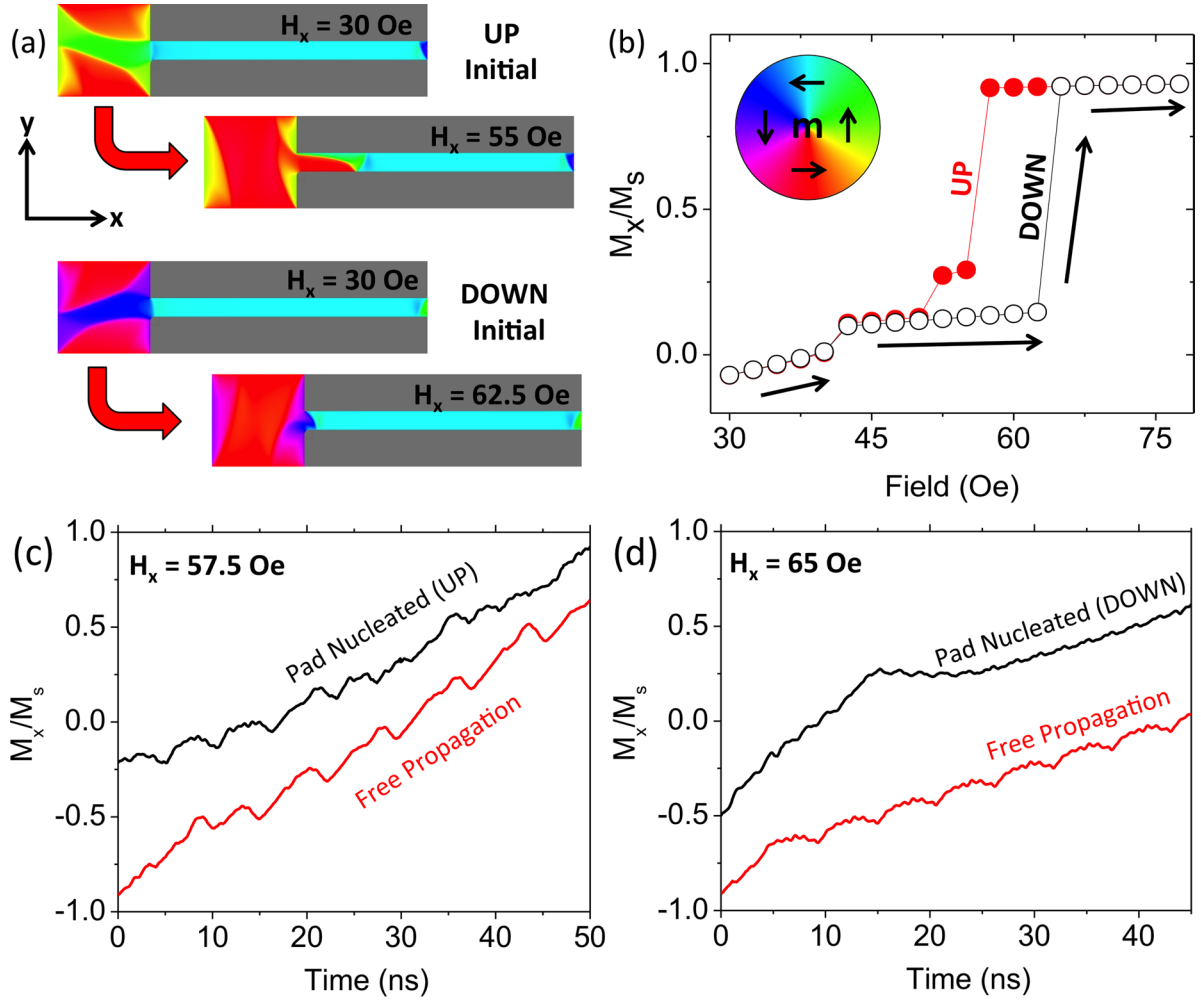
Figure 11. (a) Micromagnetically simulated states at $H = 30$ Oe and just prior to DW injection in a 6 μm long nanowire connected to a 2 μm $\times$ 2 μm nucleation pad. The nanowires had $w = 400$ nm and $t = 20$ nm. (b) Quasi-static simulations of domain wall injection for both the 'UP' and 'DOWN' initial states. (c) Comparison of magnetisation dynamics between domain walls injected from the 'UP' initial state and domain walls propagating freely at the same field ($H = 57.5$ Oe). (d) Equivalent plots for domain walls injected from the 'DOWN' state and propagating at ($H = 65$ Oe).

with current lines (figure 9(b)). As expected the IFDs from the nucleation pad were much wider ($\sigma = 4$ Oe) than those from the current lines ($\sigma = 0.5$ Oe), with finite width of the current line distributions being attributable to a combination of trigger jitter and the accuracy of our automated analysis of the FMOKE data. More surprising was the dramatic reduction of pinning/depinning stochasticity when current lines were used to inject the DWs, which was marked enough that it was clearly visible in the DFD histograms. For all of the devices with nucleation pads a number of switching modes were observed, with at least two being well populated in each device. Furthermore, substantial overlap between the IFDs and DFDs was observed, indicating a large number of DWs passing through the defect sites without pinning. In contrast to this, in all of the devices with current lines a single depinning mode dominated, with other modes being populated by just a few switching events. There was also very little overlap between the IFDs and DFDs, suggesting a pinning probability close to unity. These observations are borne out by the quantitative metrics measured from the DFDs with the average pinning probability and DFD standard deviation being 0.80

and 21 Oe for the nucleation pad nanowires versus 0.99 and 9 Oe for the current line devices. Thus, moving to a more controlled injection method clearly reduced the stochasticity of DW pinning/depinning.

In the simulations shown earlier in figure 5(b) it can be clearly seen that the period of Walker breakdown transformations decreased rapidly as the applied field is increased. Thus, one possible explanation for the larger stochasticity of the DWs injected from the nucleation pads is that the larger IFDs in these devices resulted in DWs arriving at a wider variety of points in their transformation cycles than in the current line devices, where the dynamics of the DWs were expected to be similar in all cases.

To probe this explanation we selected a single nanowire from the current line set and used it to emulate the IFD of a nanowire from the nucleation pad set by taking 50 single shot measurements at injection fields between 37.5 Oe and 54 Oe in 1.5 Oe increments. A composite DFD was then assembled by weighting the DFDs from each injection field by the appropriate value from the nucleation pad nanowire's IFD. Data from these measurements is presented in figure 10 and shows

J. Phys. D: Appl. Phys. **50** (2017) 084006

T J Hayward and K A Omari

that even when operating over a relatively wide range of injection fields the current line injection method still produced less stochastic behaviour, with an average pinning probability of 1 and DFD standard deviation of 4 Oe versus 0.7 and 22 Oe for the nucleation pad nanowire. This suggests that injecting via a current line produces fundamentally different DW behaviours than injecting via a nucleation pad.

Probing the precise physical origins of the effects described above presents a challenging problem. Accurate dynamic simulations of extended nanowires with large-scale injection pads are beyond the capabilities of current computational hardware, and fast nanomagnetic imaging techniques cannot be applied effectively to stochastic systems. Instead, micromagnetic simulations of a shorter nanowire (6 μm) connected to smaller nucleation pad (2 μm $\times$ 2 μm) were performed in order to investigate how the processes of injection modified DW dynamics in comparison to that during free-propagation, which we postulated to closely resemble the cases where DWs were ballistically injected by the current lines. The geometry of the simulated nanowire is shown in figure 11(a). In order to replicate the effects of imperfections in the experimental devices a small asymmetry was introduced at the lower edge of the junction between the pad and the nanowire.

We initialised the nanowire in one of two states shown in figure 11(a). These differed by whether the y-component of the pad's magnetisation lay along $+y$ ('UP') or $-y$ ('DOWN'). We then performed quasi-static simulations to determine the applied field at which DWs were injected from the pad into the nanowire (figure 11(b)). For the 'UP' initial state injection of a ACW VDW occurred at $H = 57.5$ Oe and was preceded by the growth of a reversed domain ~1 μm into the nanowire. For the 'DOWN' initial state a CW VDW was injected at a higher field of $H = 65$ Oe, and occurred abruptly at the junction with the pad. The differences between the injection fields and processes for the two initial states may be attributed directly to the asymmetry at the junction between the pad and nanowire.

Having determined the injection fields for the two initial states we then performed dynamic simulations ($\alpha = 0.01$) of the DWs' injection and subsequent propagation along the nanowire. Plots of M_x/M_s versus time for the simulations initialised in both the 'UP' and 'DOWN' states are shown in figures 11(c) and (d) along with equivalent simulations of free DW propagation at the same applied fields. In both cases, clear differences between the pad injection and free propagation dynamics can be observed. For the free propagation dynamics, both plots show regular oscillations, corresponding to regular transformations of the DWs structure. In contrast to this, the plots for the DWs injected from pads show both short term (figure 11(c)) and longer term (figure 11(d)) irregularities in the dynamics of the DWs.

To investigate these irregularities in more detail we analysed the simulated transformation cycles of the propagating DWs. Figure 12 contrasts the magnetisation dynamics observed for the 'UP' configuration with those for free propagation at $H = 57.5$ Oe. For free propagation the vortex core 'bounced' regularly back and forth between the upper and lower edges of the nanowire, thus forming pseudo-TDWs at the extremes of its motion (figure 12(a)). However, when depinning from the
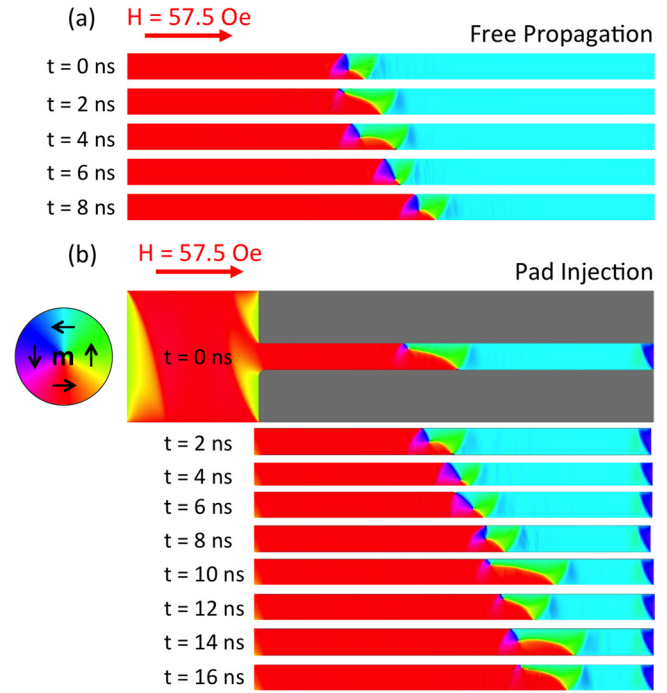

Figure 12. (a) Micromagnetic simulations of domain wall propagation at $H = 57.5$ Oe in a $t = 20$ nm, $w = 400$ nm nanowire. (b) Simulation of a domain wall injecting from a pad at the same field. The pad is only shown for the $t = 0$ ns configuration. The configurations presented have been chosen to highlight short-term variations in the domain wall's transformation cycles.

pad, the DW showed complex and irregular dynamics, where the distance the vortex core moved from the top edge of the nanowire varied from one cycle to the next (figure 12(b)), thus producing the short term irregularities in the data shown in figure 11(c).

Figure 13 makes a similar comparison between dynamics observed for the 'DOWN' state with those for free propagation at $H = 65$ Oe. For free propagation at this field the vortex core again 'bounced' from the top edge of the wire, but with smaller oscillation amplitude than at the lower field (figure 13(a)). The dynamics observed for the pad injection differed substantially from this, with the leading edge of the DW initially propagating rapidly to form a highly elongated state, before stopping until the trailing edge caught up, reinitiating forward motion, thus producing the long term irregularities in the data shown in figure 11(d). Videos showing the magnetisation dynamics observed in all four simulations may be found in this paper's supplementary material (stacks.iop.org/JPhysD/50/084006/mmedia).

The simulations presented here provide a strong indication that the details of the Walker breakdown dynamics exhibited by DWs may be modified from those expected for free propagation by the magnetisation history of the system. While it is impossible to directly correlate the simulated dynamics with those occurring in the experimentally characterised nanowires, we propose that the enhanced stochasticity observed for DWs injected from nucleation pads may result from similar effects: For example, different modes of injection from the nucleation pads may lead to substantially different DW
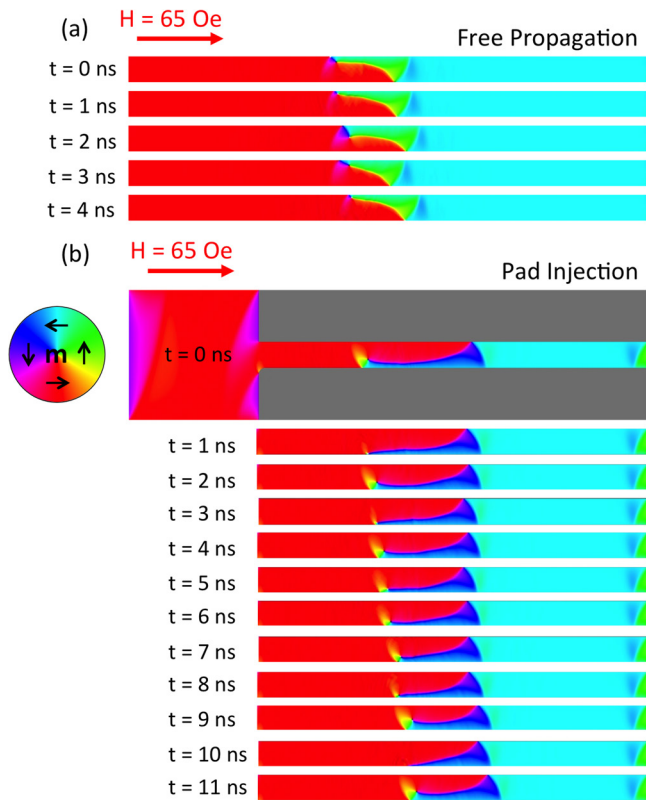
J. Phys. D: Appl. Phys. **50** (2017) 084006

T J Hayward and K A Omari

Figure 13. (a) Micromagnetic simulations of domain wall propagation at $H = 65$ Oe in a $t = 20$ nm, $w = 400$ nm nanowire. (b) Simulation of a domain wall injecting from a pad at the same field. The pad is only shown for the $t = 0$ nm configuration. The configurations presented have been chosen to highlight the initial elongation of the domain wall, and subsequent stalling in its forward motion. We note that, although the freely propagating DW has opposite chirality (ACW) to that injected from the pad (CW), the symmetry of pad-less wire means that dynamics in it will be equivalent for ACW and CW VDWs.

dynamics, even in cases where the injection fields are very similar, thus producing a wider array of pinned states at defect sites. This suggests a new layer of complexity in the stochastic pinning/depinning of DWs, where the response of the system not only depends on its magnetisation history (i.e. the chirality and structure of DWs at the point of injection) and the free propagation dynamics of DWs (i.e. the form of DW transformations), but also on complex interplay between the two. Practically, the sheer complexity of these effects may make it impossible to understand and predict stochastic effects at a quantitative level.

Conclusions

In this paper we have used a combination of experimental measurements and micromagnetic simulations to probe the stochastic pinning and depinning of DWs in soft ferromagnetic nanowires. By using FMOKE measurements to characterise a large range of defect and nanowire geometries we demonstrated these effects are a generalised behaviour of these systems, with only a minority of geometries exhibiting both reliable DW pinning and single mode depinning field

distributions. We then used measurements of single and double notch shaped defects to demonstrate that stochastic pinning/depinning effects cannot be caused only by variations in the chirality of the DWs injected into a nanowire (i.e. its magnetisation history), but must also be related to the dynamics of DWs propagating above the Walker breakdown field. Having described the dynamical origins of stochastic DW behaviours we then presented a new micromagnetic-based modelling protocol capable of explaining the complex depinning field distributions produced by defect sites at a qualitative level, and successfully applied this technique to several of the experimental measured nanowires.

We then probed how the quantitative degree of stochasticity observed at defect sites depended on the method used to inject DWs into nanowires, showing that DWs injected from nucleation pads exhibited substantially higher levels of stochasticity than those nucleated by current pulses passed through orthogonal current lines. Further experiments indicated that these differences were intrinsic to the injection processes, rather than simply due to the larger injection field distributions of the nucleation pads. Dynamical micromagnetic simulations were then used to show how the Walker breakdown transformations exhibited by DWs injected from nucleation pads were substantially more complex and irregular than those observed when DWs were allowed to propagate freely under equivalent applied fields, thus potentially creating enhanced levels of stochasticity. The complexity of these effects implies that extending our qualitative predictions of DFDs to a quantitative level may be almost impossible,

Together our results show that stochastic DW pinning and depinning is caused by a complex range of factors that not only include the magnetisation history of the nanowires and the propagation dynamics of DWs within them, but also a complex interplay between the two. Furthermore, other studies have demonstrated how thermal excitations can directly affect DW depinning [27] and propagation dynamics [11], and these effects may add further layers complexity on top of those we have identified here. In combination, our studies reinforce the view that, even in simple pseudo-one dimensional nanomagnets, DWs must be considered as complex, dynamically evolving objects rather than simple quasi-particles.

Acknowledgments

References

[1] Hrkac G, Dean J and Allwood D A 2011 *Phil. Trans. R. Soc.* A **369** 3214
[2] Allwood D A, Xiong G, Faulkner C C, Atkinson D, Petit D and Cowburn R P 2005 *Science* **309** 1688
[3] Omari K A and Hayward T J 2014 *Phys. Rev. Appl.* **2** 044001
[4] Parkin S S P, Hayashi M and Thomas L 2008 *Science* **320** 190–4
[5] Parkin S S P and Yang S-H 2015 *Nat. Nanotechnol.* **10** 195

[6] Beach G S D, Nistor C, Knutson C, Tsoi M and Erskine J L 2005 *Nat. Mater.* **4** 741

[7] Vernier N, Allwood D A, Atkinson D, Cooke M D and Cowburn R P 2004 *Europhys. Lett.* **65** 526

[8] Diegel M, Glathe S, Mattheis R, Scherzinger M and Halder E 2009 *IEEE Trans. Magn.* **45** 3792

[9] Hayashi M, Thomas L, Rettner C, Moriya R, Bazaliy Y B and Parkin S S P 2007 *Phys. Rev. Lett.* **98** 037204

[10] Bryan M T, Schrefl T and Allwood D A 2007 *Appl. Phys. Lett.* **91** 142502

[11] Hayward T J 2015 *Sci. Rep.* **5** 13279

[12] Tanigawa H, Koyama T, Bartkowiak M, Kasai S, Kobayashi K, Ono T and Nakatani Y 2008 *Phys. Rev. Lett.* **101** 207203

[13] Muñoz M and Prieto J L 2011 *Nat. Commun.* **2** 562

[14] Hayashi M, Thomas L, Rettner C, Moriya R, Jiang X and Parkin S S P 2006 *Phys. Rev. Lett.* **97** 207205

[15] Im M-Y, Bocklage L, Fischer P and Meier G 2009 *Phys. Rev. Lett.* **102** 147204

[16] Pi U-H, Cho Y-J, Bae J-Y, Lee S-C, Seo S, Kim W, Moon J-H, Lee K-J and Lee H-W 2011 *Phys. Rev.* B **84** 024426

[17] Briones J, Montainge F, Hehn M and Lacour D 2011 *Phys. Rev.* B **83** 060401

[18] Akerman J, Muñoz M, Maicas M and Prieto J L 2014 *J. Appl. Phys.* **115** 183909

[19] Ahn S-M, Moon K-W, Kim D-H and Choe S-B 2009 *Appl. Phys. Lett.* **95** 152506

[20] Lewis E R, Petit D, O'Brien L, Jausovec A-V, Zeng H T, Read D E and Cowburn R P 2011 *Appl. Phys. Lett.* **98** 042502

[21] Zeissler K, Walton S K, Ladak S, Read D E, Tyliszczak T, Cohen L F and Branford W R 2013 *Sci. Rep.* **3** 1252

[22] Pushp A, Phung T, Rettner C, Hughes B P, Yang S H, Thomas L and Parkin S S P 2013 *Nat. Phys.* **9** 505

[23] Vansteenkiste A, Leliaert J, Dvornik M, Helsen M, Garcia-Sanchez F and Van Waeyenberge B 2014 *AIP Adv.* **4** 107133

[24] Laufenburg M *et al* 2006 *Appl. Phys. Lett.* **88** 052507

[25] Donahue M J and Porter D G 1999 OOMMF User's Guide, Version 1.0 *Interagency Report NISTIR* 6376 National Institute of Standards and Technology, Gaithersburg, MD

[26] Schryer N L and Walker L R 1974 *J. Appl. Phys.* **45** 5406

[27] Wuth C, Lendecke P and Meier G 2012 *J. Phys.: Condens. Matter* **24** 024207